

JOANNA PSZONKA¹, BERNHARD SCHULZ²

SEM Automated Mineralogy applied for the quantification of mineral and textural sorting in submarine sediment gravity flows

Introduction

SEM Automated Mineralogy (SEM-AM) provides a particle characterisation incorporating quantitative mineral liberation analysis (MLA) which initially was designed as a tool in optimization in mineral processing (Fandrich et al. 2007; Ford et al. 2011; Kelvin et al. 2011). The features of SEM-AM are increasingly applied in geosciences beyond this purpose (e.g. Sylvester 2012; Schulz et al. 2020), because the automated data extraction provides highly representative measurement statistics and reduces an operator bias comparing with tedious manual techniques (Blannin et al. 2021). The available SEM-AM systems are based on a scanning electron microscope (SEM) equipped with backscattered electron detector (BSE) and an energy dispersive X-ray spectrometer (EDS) and computer software platforms that

✉ Corresponding Author: Joanna Pszonka; e-mail: jpszonka@min-pan.krakow.pl

¹ Mineral and Energy Economy Research Institute, Polish Academy of Sciences, Kraków, Poland;

ORCID iD: 0000-0002-2776-0224; e-mail: jpszonka@min-pan.krakow.pl

² Freiberg University of Mining and Technology, Department of Economic Geology and Petrology, Germany;

ORCID iD: 0000-0001-5003-3431; e-mail: bernhard.schulz@mineral.tu-freiberg.de



© 2022. The Author(s). This is an open-access article distributed under the terms of the Creative Commons Attribution-ShareAlike International License (CC BY-SA 4.0, <http://creativecommons.org/licenses/by-sa/4.0/>), which permits use, distribution, and reproduction in any medium, provided that the Article is properly cited.

automates both measurements and analysis (Gu and Napier-Munn 1997; Gu 2003; Schulz et al. 2020). High resolution BSE images allow the distinction of very fine-grained particulate materials, at the scale of micrometres. Imaging is fundamental in this system because the backscattered electron (BSE) image analysis determines grain boundaries and locations for X-ray spectral acquisition that allows for discrimination of particles, in this case mineral phases.

This paper shows how SEM-based automated mineralogical methods incorporating the mineral liberation analysis can be applied for the study of mineralogical and textural sediment sorting during depositional processes. Research into sediment sorting characteristics poses a major challenge (Sylvester and Lowe 2004) because it involves tedious measurements to produce statistically significant data. On the other hand, sediment sorting analysis is crucial in understanding of complexity of depositional process dynamics, especially in submarine environments where inaccessible location and random occurrence restrict their direct monitoring. As an example to demonstrate SEM-AM potential in this area, the Cergowa sandstones (Lower Oligocene) from the Outer Carpathians of Poland (Figure 1) were chosen, which are deposits of submarine density flows, possibly initiated by hyperpycnal effluents (Pszonka et al. 2019).

1. Material and equipment

1.1. Material

The Cergowa sandstones were sampled in their proximal facies at the Lipowica quarry, (Figure 1; Jankowski et al. 2004; Dziadzio et al. 2006; Jankowski et al. 2012; Siemińska et al. 2018), where they mainly represent steady, high-density sediment gravity flow deposition, possibly by hyperpycnal flows (Ślącza 1971; Pszonka 2015; Pszonka et al. 2019). Fine- and very fine-grained arenites (Peszat 1984; Pszonka and Götze 2018) are the material appropriate to test high resolution imaging. The Cergowa sandstones were prepared for SEM-AM as seventeen standard, polished, carbon-coated thin sections: nine petrographic thin sections (labelled as HB1_A-C, HB2_A-C, HB3_A-C) and eight particle epoxy mounts (labelled as HM_1-8) with grains separated in tetrabromoethane ($>2.97 \text{ g/cm}^3$).

Samples for sandstone thin sections were collected from three tripartite beds (20–30 cm in thickness; Figure 2). These triplets, common in the Lipowica outcrop, were interpreted as deposits of hybrid flows (Dirnerová et al. 2012), with high-density turbidite sandstones at the base, correlated with H1 division *sensu* Haughton et al. (Haughton et al. 2009), then overlain by linked debrite H3, and finally capped by low-density turbidite sandstones H4 at the top (Figure 2). One sample was taken from each of the three structural and textural intervals of these beds to capture vertical textural and compositional variations as follows: (i) samples A represent the lower part of beds, characterized by massive or graded fine-grained



Fig. 1. Schematic geological map of the Carpathians (after Kováč et al. 1998): red dot indicates position of the Lipowica quarry measured section, sample from which were analysed with the mineral liberation analyser test. GPS coordinates of the sampled locality: 49°31'42.3" N 21°40'46.0" E

Rys. 1. Schematyczna mapa geologiczna Karpat (Kováč i in. 1998)

sandstone (H1 division; Figure 2A) sometimes with granules (H1 division; Figure 2B), (ii) samples B were collected in the middle part of beds with massive fine-grained sandstone, sometimes muddy, with mudstone clasts (H3 division; Figures 2C–D), and (iii) samples C represent upper parts of beds, composed of laminated very fine-grained sandstone and siltstone, rich in clay minerals and organic detritus, showing alternation of darker and lighter laminae (H4 division; Figures 2E–F).

Five samples for heavy mineral separates (called ‘granular samples’) were collected from very thick beds (up to 6 m) of massive and graded sandstones (Figures 3A, B and D; labelled as HM_1-5), deposited by high-density gravity flows. The next three samples (labelled HM_6-8) were taken from parallel- and cross-laminated sandstones, sometimes massive, however with much lower thickness (up to 50 cm; Figures C-D), deposited by lower density flows and under the influence of transformations between high- and low-density flows (Pszonka 2015).



Fig. 2. Fragments of tripartite beds from Lipowica, interpreted as deposits of hybrid flows *sensu* Haughton et al. (Haughton et al. 2009).

A–B. Division H1, massive or graded fine-grained sandstone, sometimes with granules, represented by samples HB1-A, HB2-A and HB3-A; C–D. Division H3, massive fine-grained sandstone, sometimes muddy, with mud clasts, represented by samples HB1_B, HB2_B and HB3_B; E–F. Division H4, laminated very fine sandstone and siltstone, rich in clay minerals and organic detritus, showing alternation of darker and lighter laminae, represented by samples HB1_C, HB2_C and HB3_C

Rys. 2. Fragmenty warstw piaskowców cergowskich interpretowanych jako warstwy hybrydowe *sensu* Haughton i in. (Haughton i in. 2009)

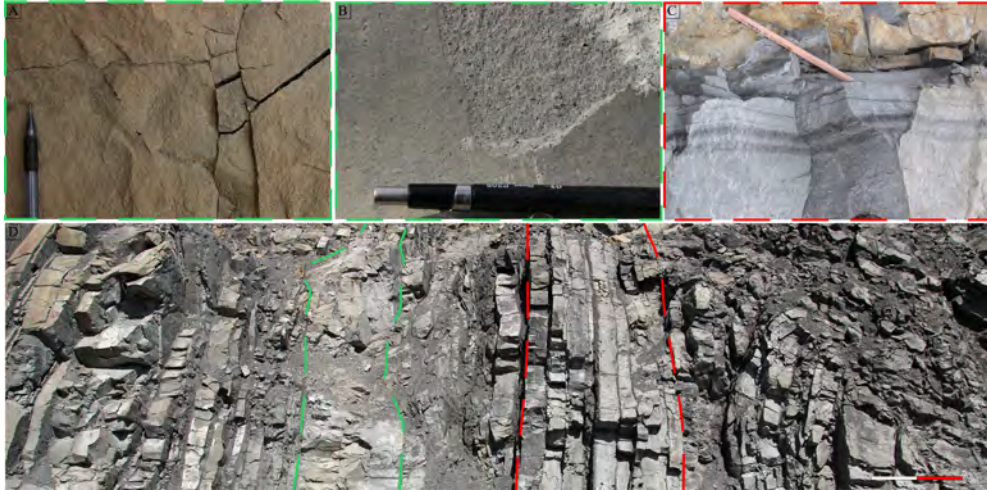


Fig. 3. A–B. Massive sandstones deposited by high-density gravity flows, represented by samples HM_1-5 (photo by Marek Wendorff). C. Parallel laminated sandstones (Td) deposited by lower density flows, represented by samples HM_6-8. D. Cergowa sandstones in the Lipowica quarry: (i) green dashed lines in the centre outline beds deposited by high-density flows, some details are shown in pictures A and B, (ii) red dash lines indicate beds deposited by lower density flows, an example is shown in pictures C. Locality of all pictures: Lipowica

Rys. 3. Przykładowe warstwy piaskowców cergowskich z Lipowicy, reprezentowane przez osady deponowane z wysokogęstościowych podmorskich prądów grawitacyjnych (rys. A, B i D) oraz z niskogęstościowych podmorskich prądów grawitacyjnych. (rys. C i D)

1.2. Equipment

Mineral liberation analyser measurements were performed at the Geometallurgy Laboratory at the Technische Universität Bergakademie Freiberg/Saxony in Germany, using the scanning electron microscope FEI Quanta 600 FEG equipped with a Bruker Quantax Dual X-Flash Detector 5010 and the automated mineralogy software version MLA 3.1.4 by FEI Company for automated data acquisition. The imaging was carried out in the backscattered electron (BSE mode) with following parameters: accelerating voltage of 15 keV, electron beam current of 10 μ A, and a working distance of 12 mm. Thin sections were measured in the XBSE (EDS single spectrum) and GXMAP (EDS spectral mapping) routines. Each X-ray analysis was made for 8 msec with a step size of 10 pixels on a 1.5×1.5 mm frame with resolution of 500×500 pixels.

2. SEM-AM functional mode

2.1. Imaging and image analysis

The development of the SEM Automated Mineralogy from early stage to the most advanced, current applications was presented in several publications, notably by (Troutmann et al. 1974; Fandrich et al. 2007; Sylvester 2012; Schulz et al. 2020).

Backscattered electrons (BSEs), reflected after elastic collisions between a SEM-generated electron beam and sample atoms, are signals used for a SEM-AM imaging. The BSE number is proportional to a sample atomic number, therefore minerals composed of heavier elements backscatter more SEM electrons and result in brighter BSE images, whereas minerals composed of lighter elements backscatter fewer electrons and appear darker.

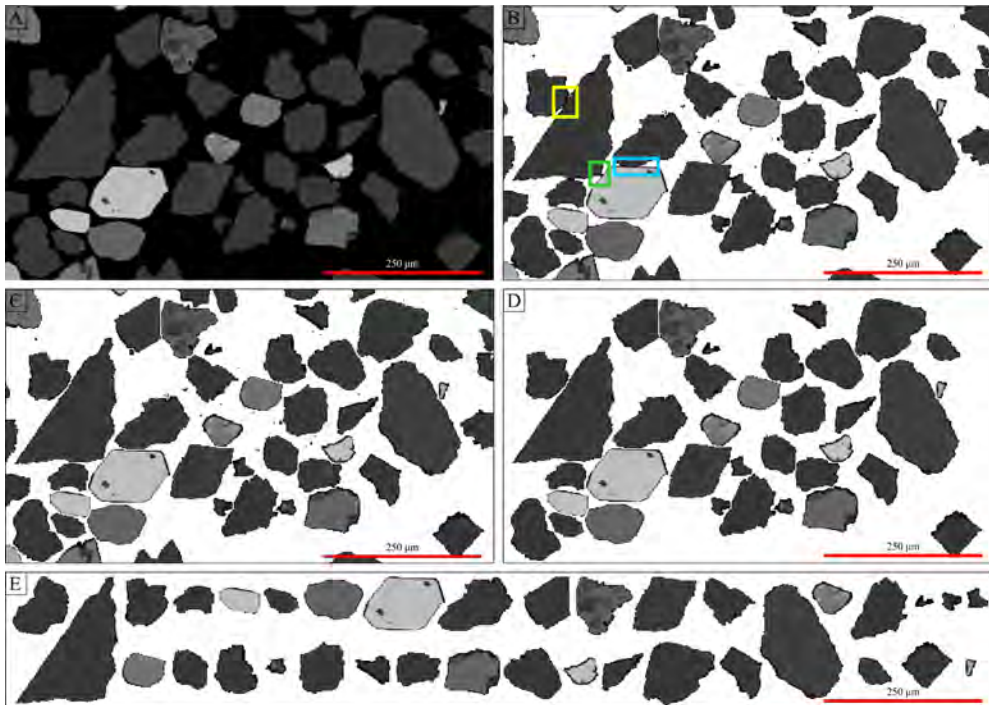


Fig. 4. Steps of the first stage in image processing, labelled as particulation procedure. A. Initial back-scattered electron (BSE) image, previous to particulation procedure. B. Background or epoxy matrix removal, labelled as background extraction. Yellow frame shows contact of particles along fractures, blue frame outlines particles with elongated contact area and green frame indicates touching particles with a small contact area. Particles are de-agglomerated by the F Low Thresh, E Steps and T Percent numerical routines. C. De-agglomeration of touching particles. D. Removal of undersized particles and particles touching the edges of a frame, labelled as clean-up. E. Final result of the particulation procedure with fully separated particles

Rys. 4. Działania wykonywane w pierwszym etapie przetwarzania obrazu w systemie MLA, nazywanym partykulacją obrazu, prezentowane na przykładzie ziaren piaskowców cergowskich

The epoxy resin used to impregnate the rock slices and mount the grains, embedding matrix with a low molecular number appears darker as most of minerals, except graphite. The SEM-AM system registers BSE images with 255 levels of a grey scale, where 0 is black and 254 white. Each mineral phase is related to a range of grey scale values, according to the molecular weight of its elemental composition. To create an image, the electron beam is scanned across the sample surface in a raster pattern. The BSE 0-254 grey scale can be calibrated with gold, copper and quartz, dependent on the sample compositional properties and scientific task.

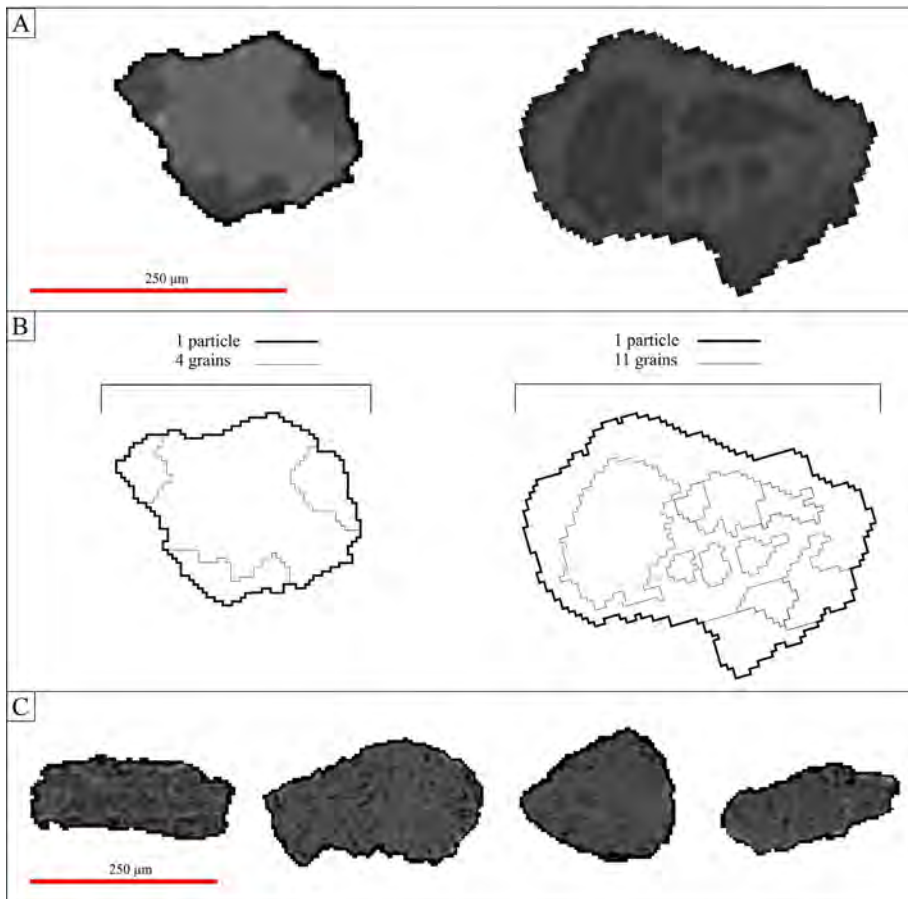


Fig. 5. The second stage of image processing, known as the segmentation procedure.

- A. Two random particles in back-scattered electron (BSE) images which underwent segmentation, delineating their mineral grains based on different values of BSE greyscale.
- B. Segmentation effect: outlines of grain boundaries. C. Grains with artefacts (internal holes and scratches, dark marginal shadow) in back-scattered electron (BSE) images previous to segmentation. The segmentation procedure eliminates the measured EDX spectra from the internal artefacts. Measured EDX spectra from the dark particle rims are labelled as a ‘Mineral 128’ and can also be deleted

Rys. 5. Drugi etap przetwarzania obrazu w systemie MLA, nazywany segmentacją obrazu, prezentowany na przykładzie ziaren piaskowców cergowskich

These high resolution BSE images (0.1–0.2 μm) of samples allow to discriminate their mineral phases through image analysis functions: particulation and segmentation. Particulation includes background removal (Figures 4A–B), de-agglomeration of linked particles (Figure 4C) and clean-up, being a removal of undersized particles and particles at edges of frames (Figure 4D). The de-agglomeration procedure controls breakage of particles along fractures (F Low Thresh), with a small contact area (T Percent) and with elongated contact area (E Steps; Figure 4B), which prevent from biased liberation results. Such prepared image (Figure 4E) is submitted to the next step in the image processing, called segmentation, which defines particle boundaries and delineates mineral grains therein based on BSE greyscale differences (Figures 5A–B). In SEM-AM terminology ‘particle’ is a sieved object that is composed of a single or several grains and ‘grain’ is a discrete mineral object in a particle (Figure 5B). The phase segmentation also eliminates particle artefacts like relief, holes, cracks, dark perimeter, uneven particle margins or halo that appear around some particles (Figure 5C).

2.2. Mineral identification

After the sample BSE image analysis, EDX spectra are collected from each delineated mineral grain to recognise a chemical composition (Figures 6A–B). Collected spectra are compared with reference spectra in order to identify a mineral phase and generate an EDX classified image by assigning unique colours to defined mineral phases (Figures 6C–D). The X-ray analysis is carried out as an EDX single point and/or EDX spectral mapping, dependent on the analytical goal. The single point EDX analysis collects spectra at the centre of each grey level area of segmented particles determined within the BSE image (Figure 7A). The EDX spectral mapping routine collects spectra by rastering over phase areas and is applied where associated minerals have the same or indistinguishable BSE grey levels (Figure 7B). The EDX spectral mapping employs a grid over particle images and collects EDX spectra at each grid point to identify mineral phases (Figure 7C). This measurement routine is also suitable for the characterisation of chemically zoned particles (e.g. Schulz et al. 2020).

2.3. Library of mineral reference spectra

Mineral classification by X-ray analysis is based on matching spectra collected on unknown grains in an analysed sample to a library of mineral reference spectra in terms of their peak-, shape-position and intensity. In the case of the MLA 2.9 and MLA 3.1 software platforms by FEI Company, this is performed by a Chi-squared difference test of the spectra; other software platforms (e.g. QEMSCAN, ZEISS, TIMA) may use alternative algorithms for the spectra classification (Schulz et al. 2020). The reference spectrum with the highest

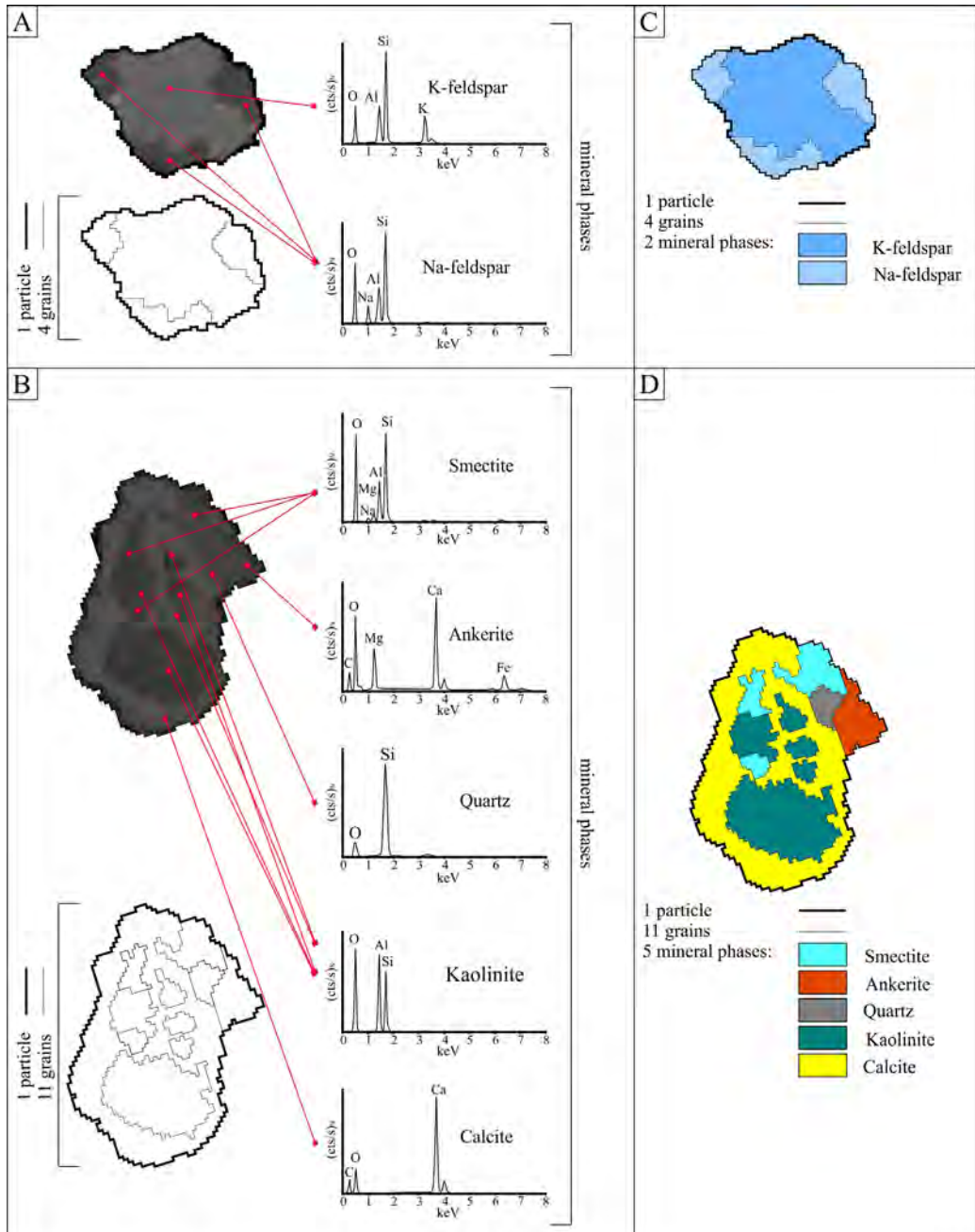


Fig. 6. Mineral identification in the SEM-AM system by EDX analysis.
 A–B. EDX spectrum collected from each mineral grain in order to recognise chemical composition.
 C–D. Assignment of unique colours to the recognised mineral phases

Rys. 6. Identyfikacja faz mineralnych w piaskowcach cergowskich za pomocą spektrometrii dyspersji energii EDX w systemie MLA

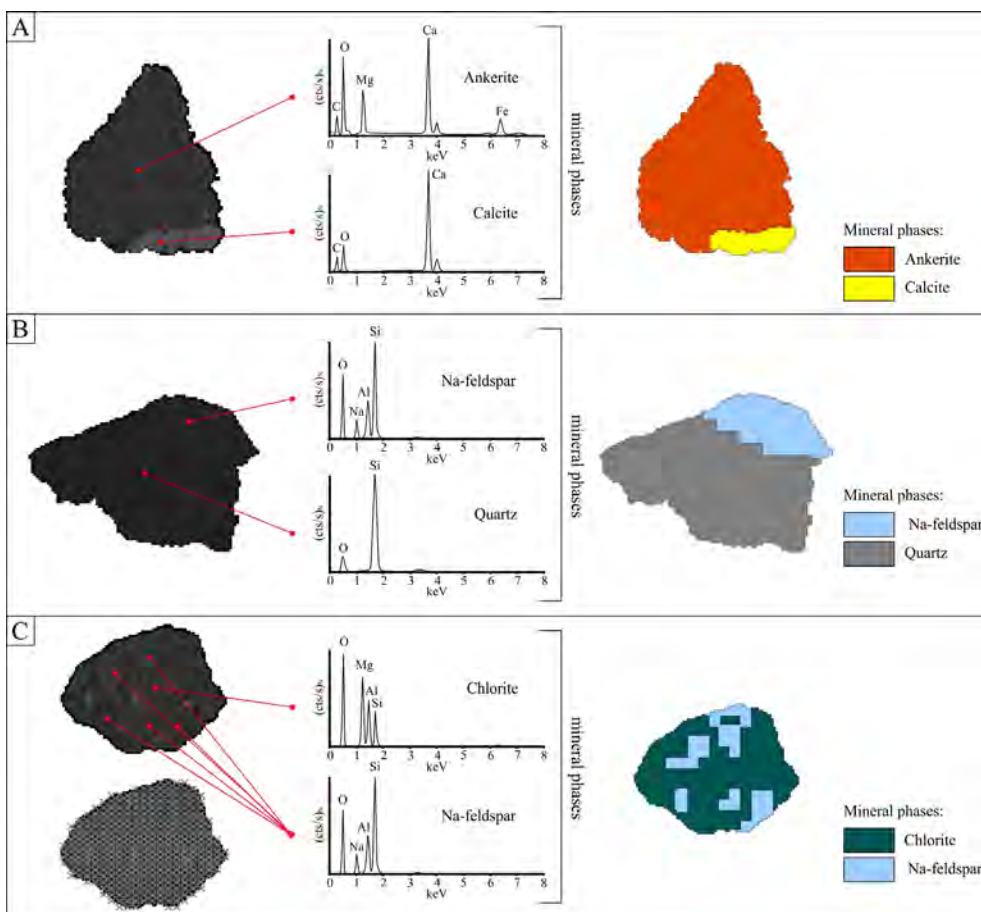


Fig. 7. Three EDX analysis techniques used to identify mineral species in the SEM-AM system.
 A. Single point EDX analysis that collects spectra at the centre of each grey level area of segmented particles.
 B. EDX spectral mapping analysis that collects spectra by rastering over larger phase areas with a pre-defined range of indistinguishable BSE grey levels.
 C. EDX spectral mapping that employs a measurement grid over complexly composed particle and collects EDX spectra at each grid point

Rys. 7. Trzy przykładowe techniki rejestracji danych zastosowane w identyfikacji faz mineralnych piaskowców cergowskich za pomocą spektrometrii dyspersji energii EDX w systemie MLA

probability is used to classify the spectrum from the sample grain. In cases where the probability is less than 80%, spectra should be collected on additional reference material. The reference spectra library is a part of a SEM-AM software platform package. However, additional mineral spectra may be collected from a given sample and identified before and during an automated run to expand the library. Then ten single X-ray spectra are collected from the same point, each with ~10000 counts. These measurements are averaged to create one reference spectrum. Some average spectra create pseudo reference spectra and they need more insight, e.g. by mean of the XRD analysis (Schulz et al. 2020). Mineral spectra without

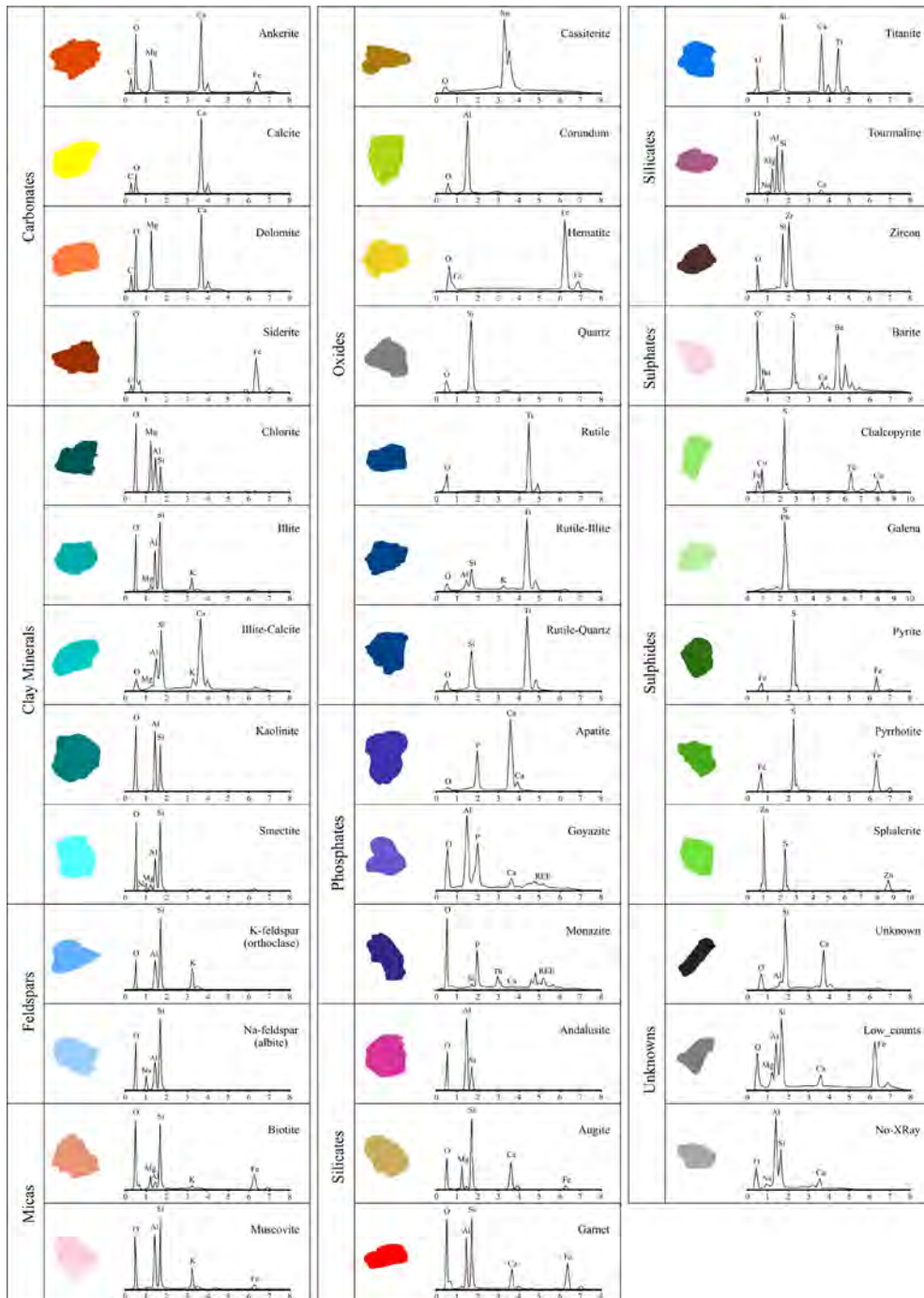


Fig. 8. Library of EDX mineral reference spectra used for mineral liberation analysis of the Cergowa sandstones
 Rys. 8. Zbiór wzorcowych widm mineralnych EDX zastosowany w zautomatyzowanej mineralogii SEM (MLA)
 piaskowców cergowskich

matching, with low counts or lack of X-ray are classified as ‘unknowns’. Moreover, some spectra gained from the dark and indistinct margin of a particle in a BSE image are deleted during the measurement by default routine of the image analysis software. Library building from the analysed samples ensures the same instrument parameters for generated reference spectra and provides accurate chemistry composition of samples (Figure 8).

2.4. Measurement modes

The SEM-AM software provides several measurement modes (e.g. Schulz et al. 2020). However, two of them are the most commonly used in particle mount and thin section studies: extended BSE liberation analysis mode (XBSE) and grain-based X-ray mapping (GXMAP). XBSE is appropriate for particle (grain) mounts (Figure 9A), where particle boundaries are discriminated by BSE imaging and identification of mineral phases is assessed by a single X-ray analysis, either over a defined area or at a single point in the grain centre (Figures 7A–B). In the case when boundaries of mineral phases cannot be segmented by BSE grey level contrast, as in petrographic thin sections (Figure 9B), a mineral identification is undertaken in the GXMAP mode with a detailed X-ray analysis on a grid pattern, known as the X-ray mapping (Figure 7C). Regardless of a sample type, granular or non-granular, X-ray data are collected in a raster pattern for series of frames stepping across particle mount or thin section (Figure 9C). The SEM-AM software joins these frames together to produce a larger mosaic panorama from the sample.

Mineral identification by the X-ray mapping in the GXMAP mode extends run times comparing with the XBSE mode because it collects more spectra to generate a mineral map. A typical run time for a XBSE analysis of particle mount is 3 hours covering 100–150 frames, whereas for a GXMAP analysis of thin section – 6 hours covering 250–300 frames or 3 hours for SEM with a FEG source. Therefore, GXMAP is used only for grains that are difficult to classify because of fine details or minerals with different chemical compositions but similar average atomic numbers (Figure 7C).

2.5. Processing

SEM-AM measurements generate false colour digital images (Figures 10A–B), coded by mineral species (Figure 10C) and linked to BSE images (Figures 10D–E) and quantitative data for each particle and grain. The SEM-AM software provides the program Image Processing for examining the BSE and X-ray data with generated digital images. This function cleans up unwanted information in images. In case of non-separation of touching particles in an automated de-agglomeration, Image Processing enables to manually separate particles by drawing a line manually by the mouse along the touching grain boundaries. All useless information, e.g. unnecessary particles or frames, may be removed likewise. Besides, the

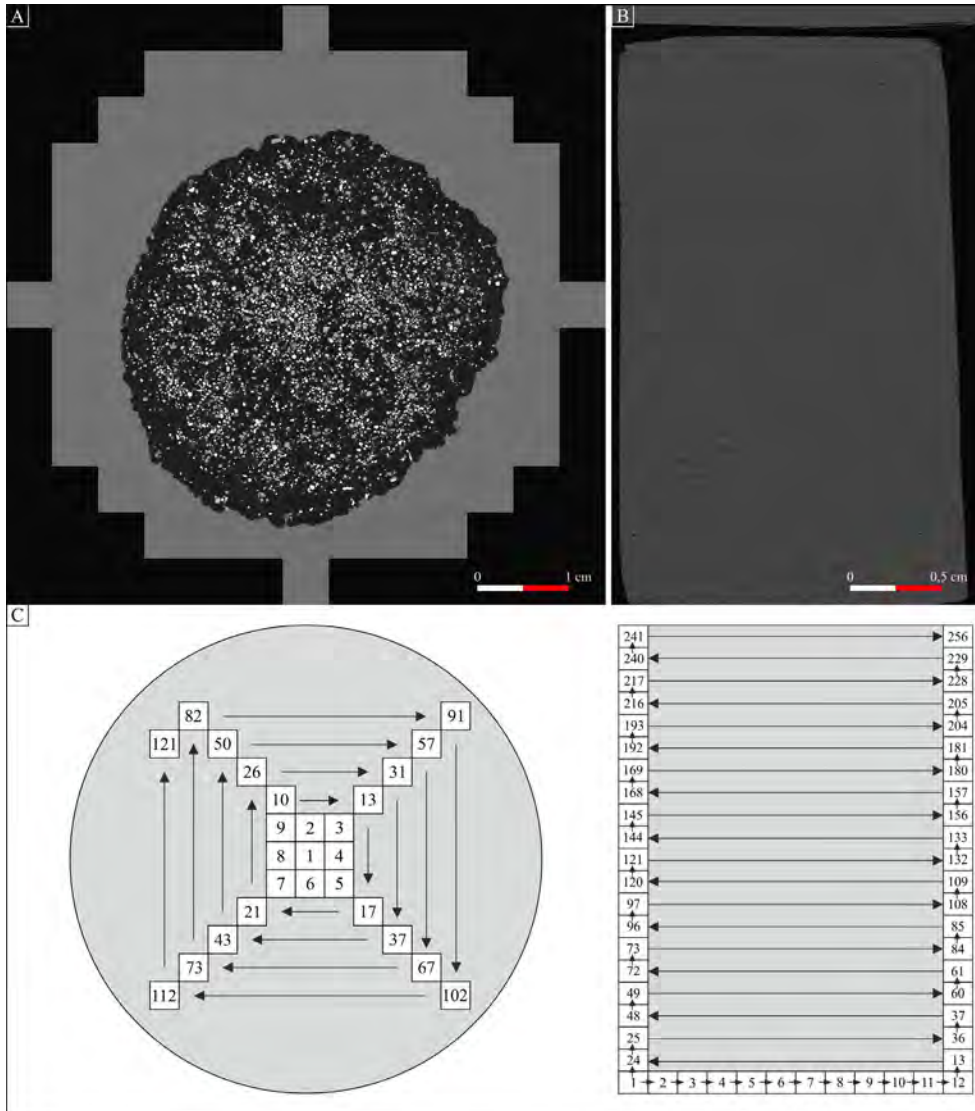


Fig. 9. A. Particle epoxy mount of the Cergowa sandstone (sample HM_7) in a back-scattered electron (BSE) image, where boundaries are discriminated and identification of mineral phases is assessed mainly by a single X-ray analysis in the extended BSE liberation analysis mode (XBSE).
 B. Thin section of the Cergowa sandstone (sample HB2_A) in back-scattered electron (BSE) image, where boundaries of mineral phases cannot be segmented by BSE grey level contrast and mineral identification is held in the grain-based EDX spectral mapping mode (GXMAP) with detailed X-ray spectrum analysis on a grid pattern.
 C. Arrangement and measurement sequence of signal measurement frame across a circular particle mount and a rectangle thin section

Rys. 9. Przykładowe preparaty piaskowców cergowskich analizowane w systemie MLA oraz technika ich pomiaru: utwardzone w żywicy wyseparowane ziarna (rys. A i C) oraz płytka cienka zglądu (rys. B i C)

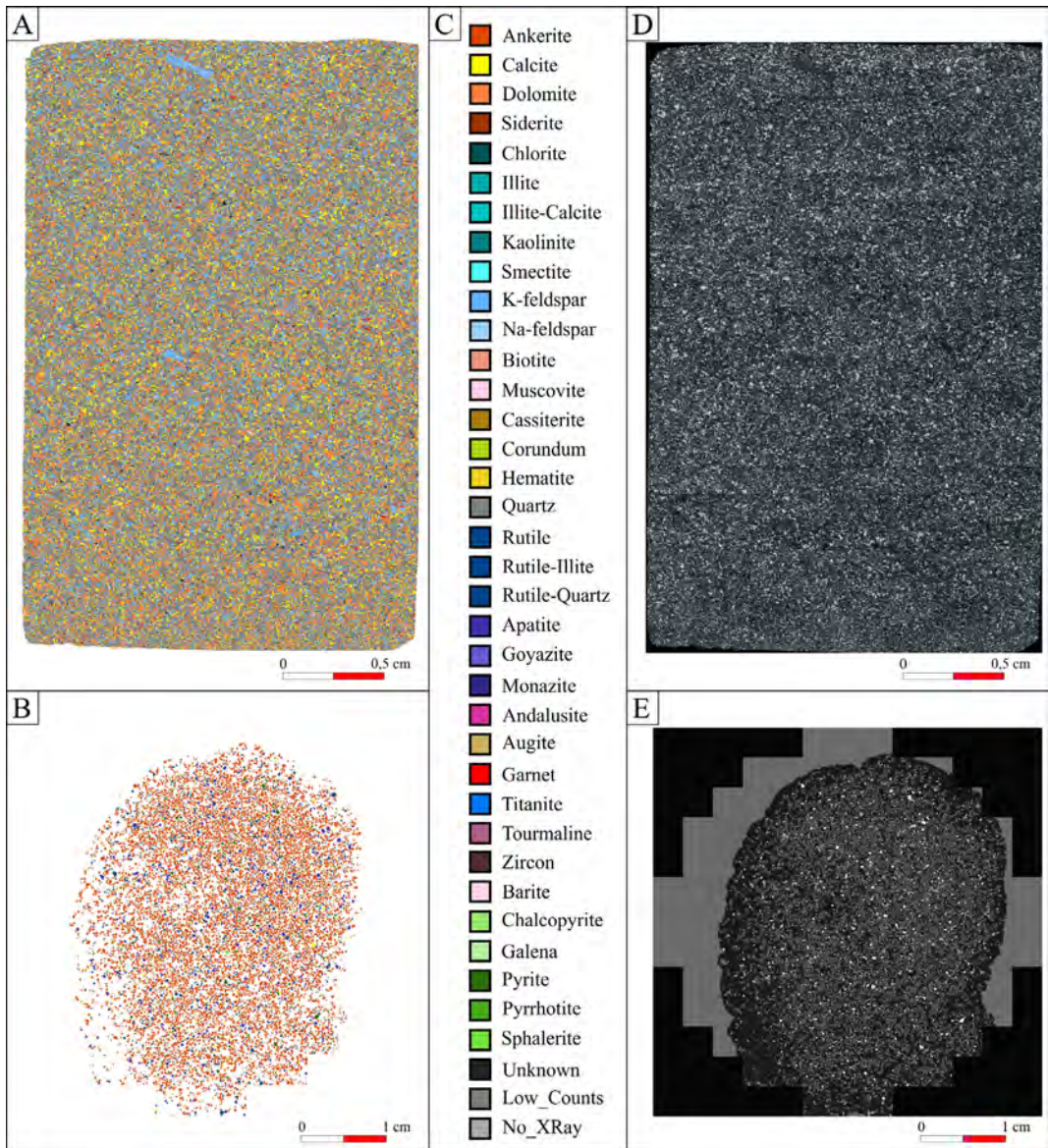


Fig. 10. A. Thin section of the Cergowa sandstone (bedding upwards) in false colour SEM-AM digital image (sample HB3_B). B. Epoxy mounted particles of the Cergowa sandstone in false colour SEM-AM digital image (sample HM_2). C. Mineral components recognised by SEM-AM in the Cergowa sandstones, coded into false colours. D. Thin section of the Cergowa sandstone in back-scattered electron (BSE) image (sample HB3_B). E. Particle epoxy mount of the Cergowa sandstones in back-scattered electron (BSE) image (sample HM_2)

Rys. 10. Płytkę cienką zglądu piaskowca cergowskiego (rys. A i D) oraz utwardzone w żywicy, wyseparowane ziarna piaskowca cergowskiego (rys. B i E) w obrazie MLA (rys. A i B) oraz SEM-BSE (rys. D i E). Rysunek C przedstawia minerały rozpoznane w piaskowcach cergowskich, zakodowane unikatowymi kolorami

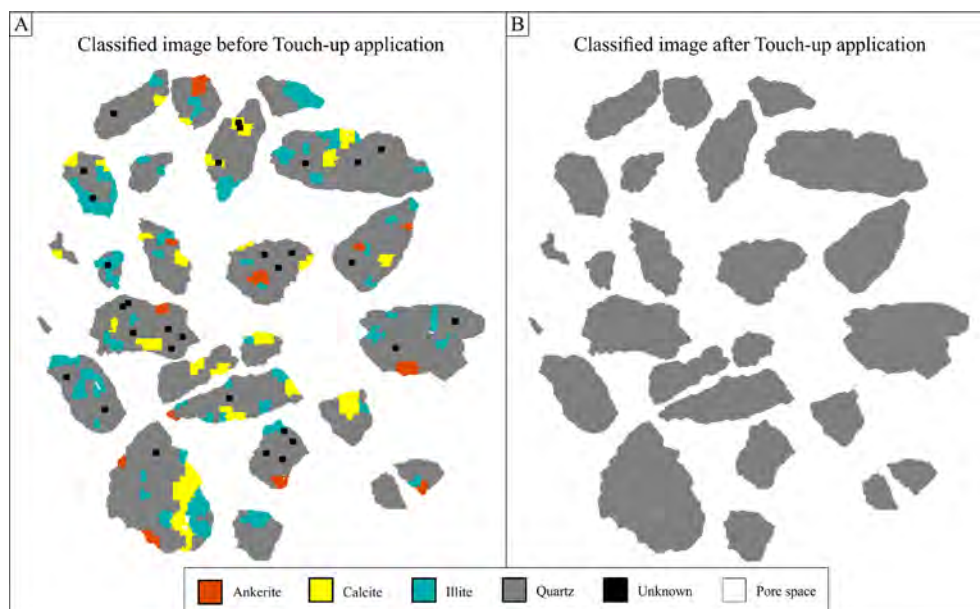


Fig. 11. Touch-up function (Touch-up 2) in SEM-AM Image Processing that converts one mineral into another.

A. Particles with some clay inclusions, pore spaces and unknown parts before the touch-up process.

B. The same particles as in A after the touch-up process

Rys. 11. Funkcja *Touch-up*, wykorzystywana do przetwarzania obrazu MLA, zaprezentowana na przykładzie piaskowca cergowskiego przy usuwaniu inkluzji mineralnych w ziarnach kwarcu

data processing program provides possibilities to convert one phase into another by three touch-up processes (Figure 11). A change of one phase enclosed within another phase into the hosting phase (Touch-up 1), and of all defined enclosed phases into each hosting phase (Touch-up 2) are applied when grains contain inclusions, pore spaces and unknown parts (Figure 11A). A Touch-up 3 can be applied to convert all dirt, metal holders and epoxy spectra into background. Image Processing offers a grouping function to combine similar mineral phases and avoid extensive reference libraries with many minor minerals or those minerals being significant for an analysis.

3. Data extraction

Pixel data in SEM-AM digital images are combined with the elemental composition and densities of identified minerals, therefore allows to generate quantitative data, including: modal mineralogy, calculated assay, elemental distribution, mineral and elemental grade recoveries, particle and mineral grain size distributions, particle density distribution, mineral associations and locking, phase specific surface area, and mineral liberation by particle composition and free surface. Granular samples with defined particle boundaries give

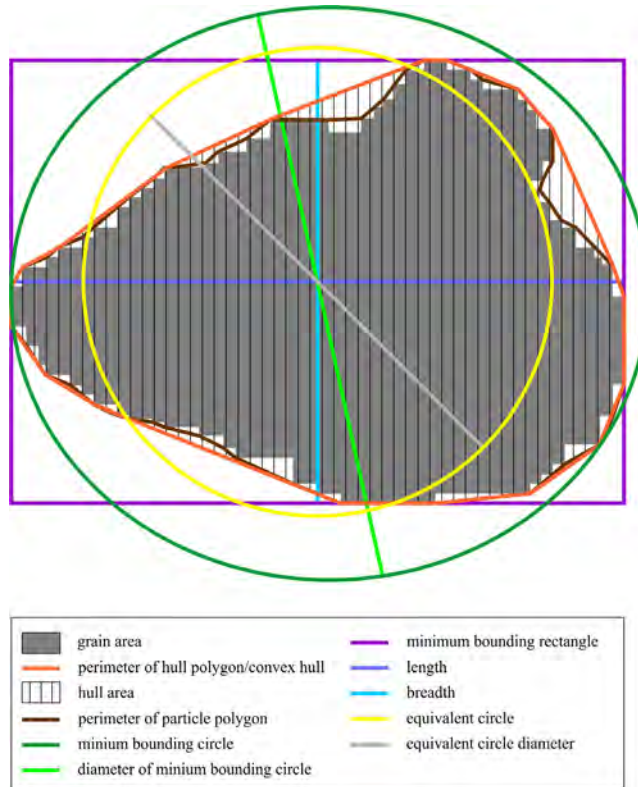


Fig. 12. Particle and grain geometrical size characterisation parameters measured in the SEM-AM system, being an output for calculation of grain shape parameters: area – area of the particle in micron squared and pixels, perimeter – surface perimeter of grain polygon, hull area – area of grain/particle convex hull in micron squared, hull perimeter – surface perimeter of grain convex hull, minimum bounding circle, diameter of minimum bounding circle, minimum bounding rectangle, length – length of minimum bounding rectangle, breadth – breadth of minimum bounding rectangle, equivalent circle, equivalent circle diameter

Rys. 12. Parametry charakteryzujące geometrię ziarna prezentowane w systemie MLA, niezbędne do analizy teksturalnej osadów

a possibility to determine not only modal mineralogy but also size distribution and shape parameters (Figure 12), such as:

- ◆ area – area of the particle in micron squared (μm^2) and pixels,
- ◆ hull area – area of grain/particle convex hull in micron squared (μm^2),
- ◆ perimeter – surface perimeter of grain polygon (μm),
- ◆ hull perimeter – surface perimeter of grain convex hull (μm),
- ◆ max span – diameter of the minimum bounding circle (μm),
- ◆ length – length of minimum bounding rectangle (μm),
- ◆ breadth – breadth of minimum bounding rectangle (μm),
- ◆ equivalent circle EC diameter – diameter of circle based on polygon area (μm),

- ◆ aspect ratio – proportion of length to breadth,
- ◆ angularity – $\Sigma([\text{Radius}] - [\text{Radius Equivalent Ellipse}]) / [\text{Radius Equivalent Ellipse}]$ in 1° increments,
- ◆ form factor – $\Sigma([\text{Radius} + 5^\circ] - [\text{Radius}]) / [\text{Radius}]$ in 1° increments.

Non-granular samples (thin sections) enable to generate and process mineralogical data, without textural information because grain boundaries of the same or similar mineralogy are not clear. This can be managed by an analysis of the complete thin section by the GXMAP spectral mapping method with the BSE background (gray color code 26) to maximum (gray color code 254). Mineral grains or particles of interest then can be electronically separated and isolated for the application of grain and particle shape and size parameters by a conversion of all matrix minerals into background with the touch-up function.

4. SEM-AM application for mineralogical and textural sorting of sediment gravity flows deposits

4.1. Non-granular samples – case study

Visual inspection of thin section images by SEM-AM (Figure 13) reveals mineral composition of analysed sandstones and grain-dominated fabric associated with intergranular carbonate and clay minerals. EDX spectra detect magnesian and ferroan varieties of calcite cement, which are essential for interpretation of diagenesis (Pszonka and Wendorff 2017). Colour maps show absence of porosity in sandstones, whereas white areas therein, classified as void spaces, result from polishing of thin sections (Figure 13). Beside the visual insight into rock composition, the DataView software also outputs modal mineralogy in quantitative terms. In order to compare the generated values, an area of the same size was cropped from each thin section image (Figure 13 – squares in the bottom row).

Proportion of calcite cement (yellow) decreases upwards in hybrid beds from 11–13% at the bottom part of the bed (H1 division) represented by samples A (HB1-A, HB2-A and HB3-A; Figure 14) to 6–8% in the middle bed (H3 division, samples HB1-B, HB2-B and HB3-B; Figure 14). Then, the calcite cement increases to 8–11% in the upper bed (H4 division, samples HB1-C, HB2-C and HB3-C; Figure 14). The similar tendency is observed in ankerite contents, that was mainly recognised as diagenetic (Pszonka and Wendorff 2017). The bottom samples (HB1-A, HB2-A and HB3-A; Figure 14) indicate 19–22% of ankerite, the middle samples (HB1-B, HB2-B and HB3-B; Figure 14) contain 13–18% of ankerite, and the upper samples (HB1-C, HB2-C and HB3-C; Figure 14) again rise to 19–22% of ankerite. This general decrease in the carbonate proportion in the middle bed, representing H3 Haughton's division (Haughton et al. 2009), seems to be an effect of reduction of intergranular pore spaces due to the smaller grain size and partial pore filling with clay

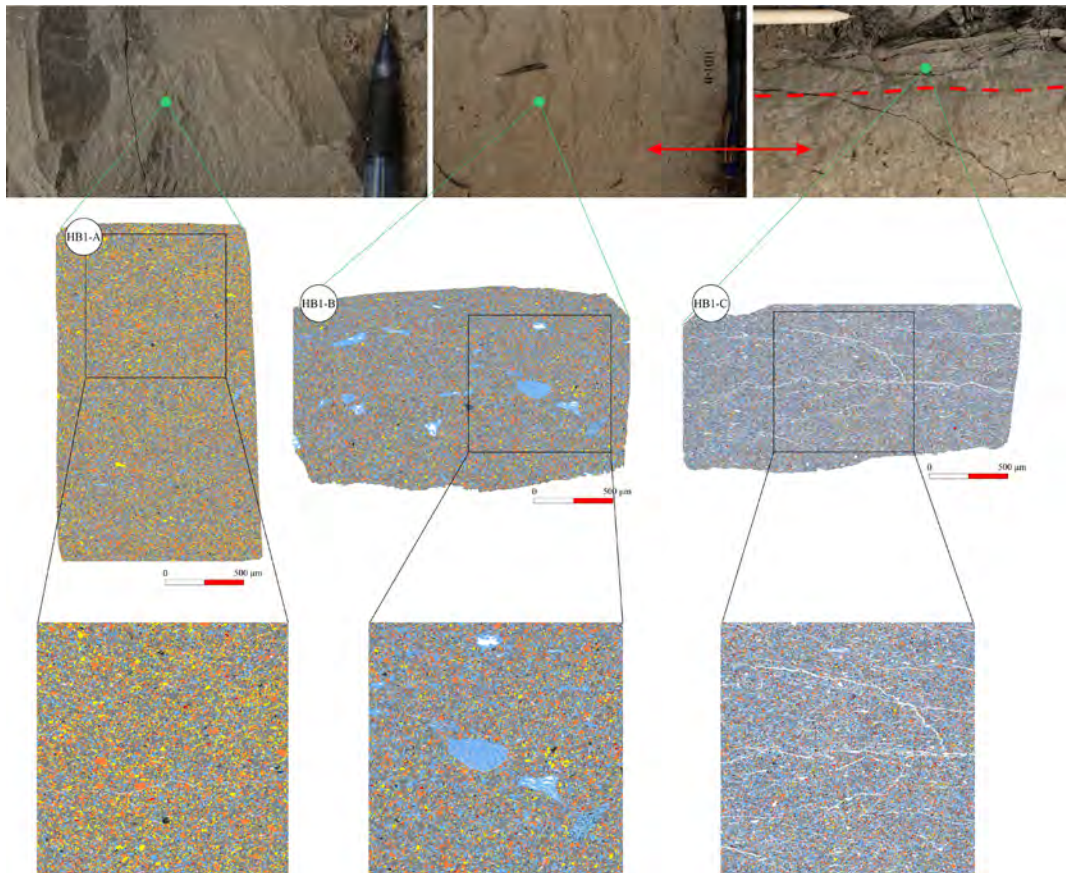


Fig. 13. HB_1-A, B and C samples presented as colour maps in the SEM-AM images (middle row) with their cut-out fragments (each of the same size, needed to compare generated values – lower row) and linked with pictures of beds from which these samples were collected (upper row). Minerals are coded into false colours according to the list of minerals in Figure 10C. Sample HB_1A represents H1 division *sensu* Haughton et al. (2009), sample HB_1B – H3 division, and sample HB_1C – H4 division. Red arrows indicate H3 division

Rys. 13. Fragmenty warstwy hybridowej piaskowców cergowskich z Lipowicy, reprezentujące interwały H1, H3 i H4 *sensu* Haughton i in. (2009), skąd pobrano materiał do analizy SEM-AM oraz obrazy MLA tych próbek

minerals (blue). Higher clay amount there contributed to the transformation of high-density turbidity current, depositing lowermost parts of hybrid beds (A samples, H1 division), into cohesive or semi-cohesive state (B samples, H3 division; Figures 2C and D). Minor occurrence of mudstone clasts in the H1 division does not alter general mineral composition of the sandstone and its depositional structures, so is insufficient to modify flow behaviour.

Moreover, quartz that constitutes the main component of the Cergowa sandstone framework grains, indicates close relations in proportion as carbonates, i.e.: bottom samples

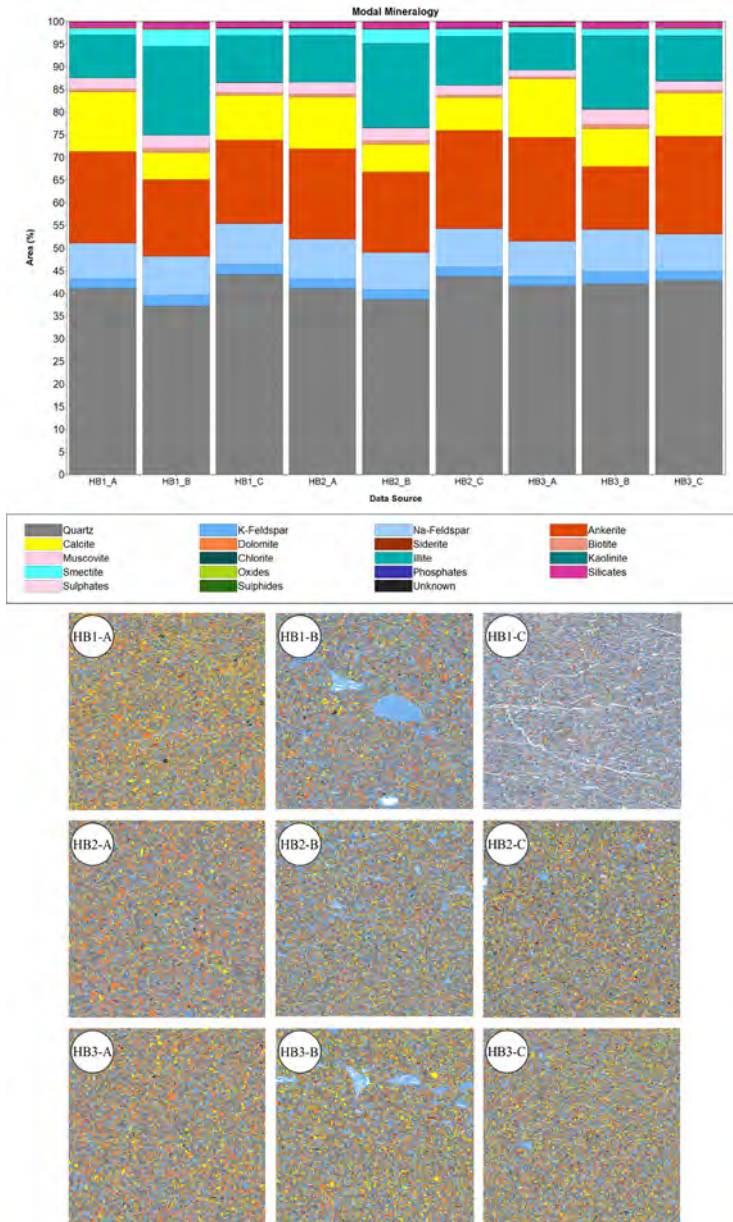


Fig. 14. Modal mineral composition of samples (A-C) collected from 3 hybrid beds HB1, HB2 and HB3, in the form of a diagram generated in the SEM-AM system. Each column with sample modal mineralogy is linked to the cut-out area, where the data were generated. Samples A were collected from bottom parts of beds HB1, HB2 and HB3 that represent H1 division *sensu* Haughton et al. (2009), samples B were collected from middle parts of beds HB1-3 that represent H3 division, and samples C were collected from upper parts of HB1-3 beds, representing H4 division

Rys. 14. Modalny skład mineralny próbek pobranych z trzech warstw hybrydowych (HB1, HB2 i HB3) piaskowców cergowskich z Lipowicy, *sensu* Haughton i in. (2009) oraz obrazy MLA analizowanych próbek (po trzy próbki: A, B i C z każdej warstwy hybrydowej)

(HB1-A, HB2-A and HB3-A; Figure 14) show ~42% of quartz, middle samples (samples HB1-B, HB2-B and HB3-B; Figure 14) decrease to 37–42% in quartz, and in upper samples (samples HB1-C, HB2-C and HB3-C; Figure 14) quartz increases to 43–44%. Therefore, a transformation of a flow statement from turbulent into cohesive not only hinders possibilities for cement development, but also depletes contributions of framework grain components.

Such variations in mineral composition between samples can be observed not only within one bed, as it was presented above, indicating transformation of a deposition mechanism. Mineralogical differences between beds within a section reflect erosion of the source area, and the consecutive degradation of rocks differing in petrographic character. Mineralogical variations between sections within regions show transport of clastic material from different areas of a depositional basin, from proximal to distal parts. And finally, these variations between regions can indicate various source areas.

As it was shown in the data extracting section, the non-granular sample (thin-section samples) analysis does not generate detailed grain size and shape information. An accurate comparison of grain mineralogy and textural characteristics is possible when grains are separated, as it was done for samples HM_1-8.

4.2. Granular samples – case study

Granular samples (particle epoxy mounts) HM_1-5 (Figure 15), representing beds deposited by high-density flows, contain mainly ankerite. By the contrast, HM_6-8 representing beds formed by lower density flows include primarily phosphates (apatite and monazite) and silicates (andalusite, augite, garnet, titanite, tourmaline and zircon; Figure 15). However, this preparation gives a crucial possibility to detect not only mineralogy but also grain texture parameters (Table 1). Moreover, 13,000–15,000 grain measurements for each HM sample constitute statistically significant data devoid of human errors, bias and tedious manual work under the optical microscope.

Mean grain-size values are concurrent in beds deposited by high- and low-density flows, and range from 54 μm to 92 μm for the former and 51–115 μm for the latter (Table 1). However, it is to be expected that the grain size measured in beds deposited by high-density flows (samples HM_1-5), in contrast to low-density flows (samples HM_6-8), is underestimated because granular samples contain exclusively grains with density $>2.97 \text{ g/cm}^3$. Steidmann's experiments (Steidmann 1982) has shown a distinct size-density sorting during high-density flows, therefore the least transportable higher density grains come to rest first whereas the more transportable lower density grains of the same size still move on and settle later. Underestimated samples HM_1-5 do not report coarser sizes of lighter grains. The separation between heavy and light minerals was not observed in low-density flows (Steidmann 1982) thus measured grain sizes in samples HM_6-8 also reflect values of grains with density $<2.97 \text{ g/cm}^3$, which were removed during the sample preparation.

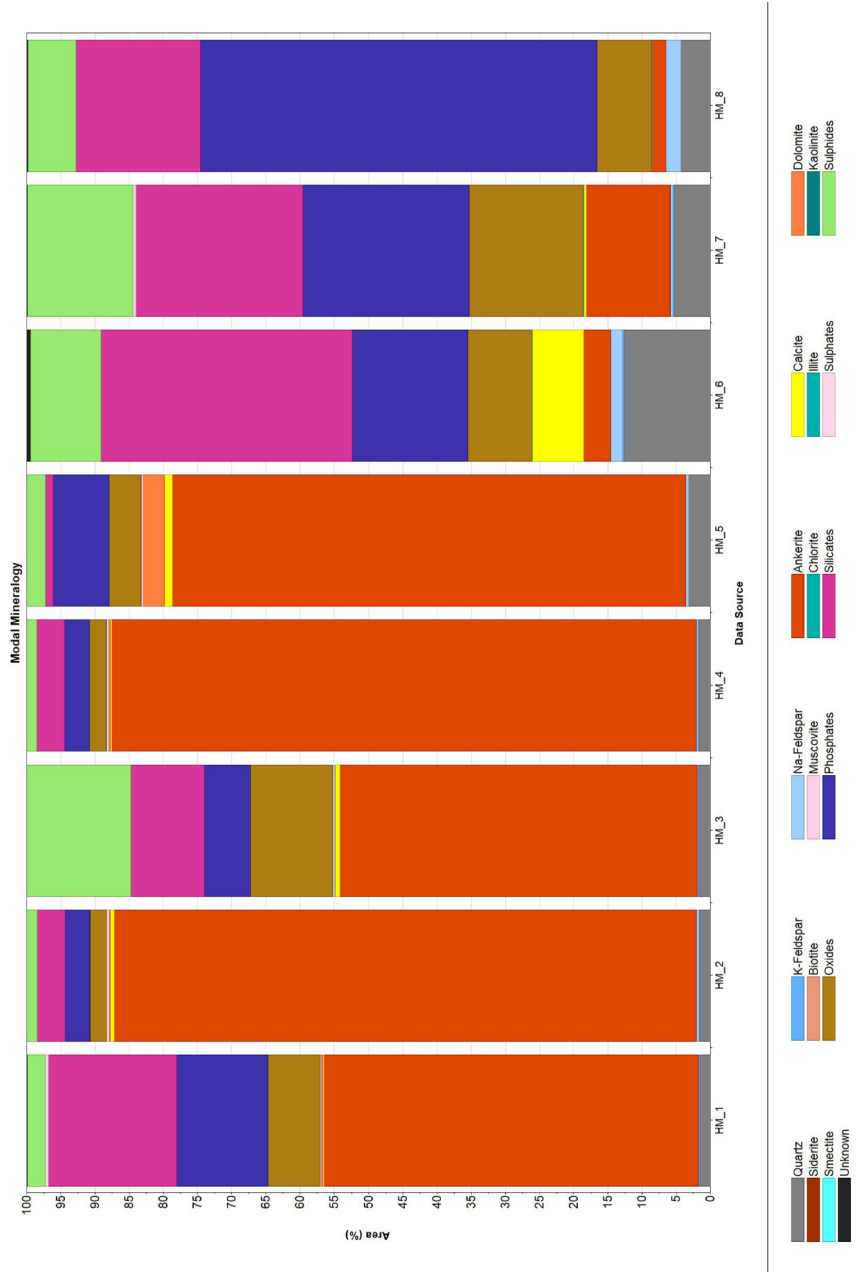


Fig. 15. Modal mineral composition in a diagram generated for samples HM_1-8. Samples HM_1-5 representing beds deposited by high-density flows, show ankerite as the main component whereas samples HM-6-8 representing beds formed by lower density flows primarily include phosphates and silicates

Rys. 15. Modalny skład mineralny wygenerowany w systemie MLA w formie histogramów dla próbek HM_1-5, reprezentujących osady zdeponowane przez wysoko-gęstościowe podmorskie splayy grawitacyjne oraz dla próbek HM_6-8, reprezentujących osady zdeponowane przez niskogęstościowe podmorskie splayy grawitacyjne

Table 1. MLA measurements (μm) of area, diameter, aspect ratio, angularity and form factor of ankerite, phosphate and silicate grains for samples HM_1-8

Tabela 1. Wyniki pomiarów [μm] wykonanych w systemie MLA powierzchni, średnicy, współczynnika proporcji, kanciastości oraz współczynnika kształtu ankerytów, fosforanów i ziaren krzemianowych obecnych w próbkach HM_1-8

Sample	Mineral grain	Area	Diameter	Aspect Ratio	Angularity	Form Factor
HM_1	Ankerite	2,984.867	58.65058	1.516018	38.27433	0.114731
	Phosphate	5,524.374	76.42298	1.466778	23.71582	0.093734
	Silicate	4,168.489	62.66569	1.692967	25.37638	0.198739
HM_2	Ankerite	4,589.976	64.21078	1.541411	36.62232	0.132487
	Phosphate	4,401.089	69.34254	1.487058	24.02526	0.108861
	Silicate	2,618.455	54.11704	1.543190	30.04963	0.164726
HM_3	Ankerite	3,576.467	64.29462	1.564088	32.74134	0.154528
	Phosphate	4,677.634	72.21378	1.487328	26.03126	0.113624
	Silicate	3,053.599	58.12825	1.535793	30.0634	0.203303
HM_4	Ankerite	3,670.285	65.03660	1.539886	33.49593	0.136326
	Phosphate	4,530.122	70.45005	1.472917	24.56188	0.102040
	Silicate	2,632.110	54.33480	1.539740	29.35350	0.151434
HM_5	Ankerite	6,217.344	83.96678	1.509449	38.33795	0.128394
	Phosphate	7,425.052	91.75827	1.457663	23.67430	0.094639
	Silicate	4,394.743	69.18729	1.673976	33.71017	0.125588
HM_6	Ankerite	3,838.573	63.80109	1.480210	27.86037	0.118099
	Phosphate	4,037.493	67.50778	1.486392	25.54124	0.092712
	Silicate	2,320.048	50.81915	1.506568	26.52697	0.093999
HM_7	Ankerite	3,426.160	62.33410	1.566249	32.81711	0.160825
	Phosphate	6,137.457	81.85833	1.431618	22.75721	0.113717
	Silicate	3,021.932	57.99746	1.537827	29.56329	0.114720
HM_8	Ankerite	10,457.300	115.09650	1.465051	37.04168	0.080220
	Phosphate	4,590.490	73.26420	1.394102	19.22060	0.077218
	Silicate	4,195.152	62.14889	1.824177	31.06949	0.155880

No differences are observed in aspect ratio of ankerite, phosphate and silicate grains (1.4–1.8, see in Table 1), which means that their sphericity is similar. On the other hand, variability in their angularity is noticeable (Table 1), namely, ankerite grains are more angular (27–38) than phosphates (19–26) and silicates (25–33). It may be assumed that detrital ankerite, typical component of high-density deposits, underwent shorter transport than phosphates and silicates that are characteristic for lower density flows. Therefore, probably angular ankerites were transported from a costal/delta zone in a low-energy shallow marine environment (Ślączka and Unrug 1976; Pszonka and Wendorff 1917), possibly by hyperpycnal flows. More rounded minerals may have originated in the mainland area, from erosion of the Silesian Ridge located to NW of the depocenter, were transported by rivers to the shoreline and then mainly deposited by lower density flows moving better reworked material and recording minor events between hyperpycnal flows.

Conclusions

High level of automation in the SEM-AM system, the functioning of which was demonstrated in this article, enables to achieve high speed, resolution, accuracy and versatility of data extracting and processing. These unquestionable advantages contributed to the choice this system to detect mineralogical and textural grain sorting during depositional processes, on the example of Carpathian submarine density flow deposits. Granular samples provided mineralogical and textural characteristics of the analysed sandstones whereas non-granular samples (thin sections), where grain boundary determination is unclear, only modal mineralogical data. The latter could be eventually improved by application of grain and particle shape and size parameters after a targeted application of the software involving regrouping and touch-up functions.

These results allow to identify variability in grain composition and texture in order to interpret competence variations within individual flows by comparing samples from one bed, and between separate flows by comparing samples from different beds. It appears promising to correlate data with different sections and regions of this formation to recognise load differences between frontal and tail parts of flows, flow sorting during basin transport and various source areas.

Comparison of mineral density with grain size and shape parameters may point to associations between mineralogical and textural sorting during submarine transport, as it is shown by grain angularities of the Cergowa sandstones, or its totally independent processing where one type of sorting is developed by suppressing the other in the same event (Shideler et al. 1975), as in the case of grain sphericity. Significant amount of reliable SEM-AM data with reduced human errors, bias and tedious manual work is suited for statistical processing of the obtained data, therefore it seems to be essential to detect relations of mineralogical and textural sorting.

Although the test study has been carried out on ancient submarine sediments, the SEM-AM system may be applicable for all types of sediments: representing various depositional environments and also modern sedimentary systems. SEM sample chamber and relatedly appropriate sample preparation (Schulz et al. 2020) are the only limitation in the mineral liberation analysis handling.

This work was supported by the National Science Centre (NCN) [grant number DEC-2017/01/X/ST10/00048] and the statutory research of the Mineral and Energy Economy Research Institute of the Polish Academy of Sciences to JP.

REFERENCES

- Blannin et al. 2021 – Blannin, R., Frenzel, M., Tusa, L., Birtel, S., Ivascanu, P., Baker, T. and Gutzmer, J. 2021. Uncertainties in quantitative mineralogical studies using scanning electron microscope-based image analysis. *Minerals Engineering* 167, DOI: 10.1016/j.mineng.2021.106836.
- Dirnerová et al. 2012 – Dirnerová, D., Prekopová, M. and Janočko, J. 2012. Sedimentary record of the Dukla Basin (Outer Carpathians, Slovakia and Poland) and its implications for basin evolution. *Geological Quarterly* 56(3), pp. 547–560, DOI: 10.7306/gq.1039.
- Dziadzio et al. 2016 – Dziadzio, P., Matyasik, I., Garecka, M. and Szydło, A. 2016. Lower Oligocene Menilite Beds, Polish Outer Carpathians: supposed deep-sea flysch locally reinterpreted as shelfal, based on new sedimentological, micropalaeontological and organic-geochemical data. Kraków: Prace Naukowe Instytutu Nafty i Gazu, Krakow, 120 pp., DOI: 10.18668/PN2016.213.
- Fandrich et al. 2007 – Fandrich, R., Gu, Y., Burrows, D. and Moeller, K. 2007. Modern SEM-based mineral liberation analysis. *International Journal of Mineral Processing* 84, pp. 310–320, DOI: 10.1016/j.minpro.2006.07.018.
- Ford et al. 2011 – Ford, F.D., Wercholz, C.R. and Lee, A. 2011. Predicting process outcomes for Sudbury platinum-group minerals using grade-recovery modelling from Mineral Liberation Analyzer (MLA) data. *The Canadian Mineralogist* 49, pp. 1627–1642, DOI: 10.1017/canmin.49.6.1627.
- Gu, Y. 2003. Automated scanning electron microscopy based mineral liberation analysis. An introduction to JK-MRC/FEI Mineral Liberation Analyser. *Journal of Minerals and Materials Characterization and Engineering* 2, pp. 33–41, DOI: 10.4236/jmmce.2003.21003.
- Gu, Y. and Napier-Munn, T. 1997. JK/Philips mineral liberation analyzer – an introduction. Cape Town: Minerals Processing '97 Conference, pp. 2.
- Houghton et al. 2009 – Houghton, P., Davis, C., McCaffrey, W. and Barker, S. 2009. Hybrid sediment gravity flow deposits – Classification, origin and significance. *Marine and Petroleum Geology* 26(10), pp. 1900–1918, DOI: 10.1016/j.marpetgeo.2009.02.012.
- Jankowski et al. 2004 – Jankowski, L., Kopciowski, R. and Ryłko, W. 2004. Geological map of the Outer Carpathians: borderland of Poland, Ukraine and Slovakia. Warszawa: Polish Geological Institute, scale 1:200000.
- Jankowski et al. 2012 – Jankowski, L., Kopciowski, R., Ryłko, W., Danysh, V., Tsarnenko, P.N. and Hnylko, O. 2012. Lithostratigraphic correlation of the outer Carpathian borderlands of Poland, Ukraine, Slovakia and Romania. *Biuletyn Państwowego Instytutu Geologicznego* 449, pp. 87–98.
- Kelvin et al. 2011 – Kelvin, M.A., Sylvester, P.J. and Cabri, L.J. 2011. Mineralogy of rare occurrences of precious-metal-enriched massive sulfide in the Voisey's Bay Ni-Cu-Co Ovoid Deposit, Labrador, Canada. *The Canadian Mineralogist* 49, pp. 1505–1522, DOI: 10.3749/canmin.49.6.1505.
- Kovač et al. 1998 – Kovač, M., Nagymarosy, A., Oszczytko, N., Csontos, L., Ślącza, A., Marunteanu, M., Matenco, L. and Marton, E. 1998. *Palinspastic reconstruction of the Carpathian-Pannonian region during the Miocene*. [In:] Rakus, M. (ed.), *Geodynamic development of the Western Carpathians*. Bratislava: Geological Survey of Slovak Republic, Dionyz Štur Publishers, pp. 189–217.

- Peszat, C. 1984. Variability of the petrographic and mineral composition of the Cergowo sandstones against the background of their deposition conditions and diagenetic transformations (*Zmienność składu petrograficzno-mineralnego piaskowców cergowskich na tle warunków ich depozycji i przemian diagenetycznych*). *Biuletyn Państwowego Instytutu Geologicznego* 346(24), pp. 207–234 (in Polish, with English summary).
- Pszonka, J. 2015. Sedimentological study of the Cergowa Beds in the Dukla and Fore-Dukla Units of the Flysch Carpathians. *Studia, Rozprawy, Monografie* 196, 193 p. (in Polish).
- Pszonka, J. and Wendorff, M. 2017. Carbonate cements and grains in submarine fan sandstones – the Cergowa Beds (Oligocene, Carpathians of Poland) recorded by cathodoluminescence. *International Journal of Earth Sciences* 106, pp. 269–282, DOI: 10.1007/s00531-016-1318-z.
- Pszonka, J. and Götze, J. 2018 Quantitative estimate of interstitial clays in sandstones using Nomarski differential interference contrast (DIC) microscopy and image analysis. *Journal of Petroleum Science and Engineering* 161, pp. 582–289, DOI: 10.1016/j.petrol.2017.11.069.
- Pszonka et al. 2019 – Pszonka, J., Žecová, K. and Wendorff, M. 2019. Oligocene turbidite fans of the Dukla Basin: New age data from the calcareous nannofossils and paleoenvironmental conditions (Cergowa beds, Polish–Slovakian borderland). *Geologica Carpathica* 70(4), pp. 311–324, DOI: 10.2478/geoca-2019-0018.
- Schulz et al. 2020 – Schulz, B., Sandmann, D. and Gilbricht, S. 2020. SEM-Based Automated Mineralogy and its Application in Geo- and Material Sciences. *Minerals* 10, DOI: 10.3390/min10111004.
- Shideler et al. 1975 – Shideler, G.L., Ślaczka, A., Unrug, R. and Wendorff, M. 1975. Textural and mineralogical sorting relationships in Krosno Formation (Oligocene) turbidites, Polish Carpathian Mountains. *Journal of Sedimentary Petrology* 45(1), pp. 44–56.
- Siemińska et al. 2018 – Siemińska, A., Starzec, K., Godlewski, P. and Wendorff, M. 2018. Sedimentary response to tectonic uplift of the Dukla basin margin recorded at Skrzydlina – the Menilite Beds (Oligocene), Outer Carpathians, S Poland. *Geology, Geophysics and Environment* 44(2), pp. 231–244, DOI: 10.7494/geol.2018.44.2.231.
- Ślaczka, A. 1971. *The Geology of the Dukla Unit, Polish Flysch Carpathians*. Warszawa: Wydawnictwo Geologiczne 63, 97 pp. (in Polish).
- Ślaczka, A. and Unrug, R. 1976. Trends of textural and structural variation in turbidite sandstones: the Cergowa Sandstone (Oligocene, Outer Carpathians). *Annales Societatis Geologorum Poloniae* 46(1–2), pp. 55–75.
- Steidmann, J.R. 1982. Size-density sorting of sand-size spheres during deposition from bedload transport and implications concerning hydraulic equivalence. *Sedimentology* 29, pp. 877–883, DOI: 10.1111/j.1365-3091.1982.tb00090.x.
- Sylvester, P.J. 2012. Use of the Mineral Liberation Analyzer (MLA) for mineralogical studies of sediments and sedimentary rock. *Mineralogical Association of Canada, Short Course Series* 42, pp. 1–16.
- Sylvester, Z. and Lowe, D.R. 2004. Textural trends in turbidites and slurry beds from the Oligocene flysch of the Carpathians, Romania. *Sedimentology* 51, pp. 945–972, DOI: 10.1111/j.1365-3091.2004.00653.x.
- Troutmann et al. 1974 – Troutmann, S., Johnson, G.G.M., White, E.W. and Lebedzik, J. 1974. Automated quantitative SEM characterization of complex particular samples. *American Laboratory* 6, pp. 31–38.

SEM AUTOMATED MINERALOGY APPLIED FOR THE QUANTIFICATION OF MINERAL AND TEXTURAL SORTING IN SUBMARINE SEDIMENT GRAVITY FLOWS**Keywords**

scanning electron microscope, SEM Automated Mineralogy, mineral liberation analysis, depositional processes, sediment sorting, submarine gravity flows

Abstract

SEM Automated Mineralogy (SEM-AM) is an analytical system based on a scanning electron microscope (SEM) with backscattered electron detector and an energy dispersive X-ray spectrometer (EDS). This automated tool enables to quantify mineralogy, size and geometry of solid matter components. The paper presents a SEM-AM application in detection of mineralogical and textural sediment sorting on the example of a submarine gravity flow record from the Cergowa sandstones (Lower Oligocene) in the Polish Outer Carpathians. Analysis of high quality backscattered electron (BSE) imagery in combination with EDX spectra discriminates mineral phases in polished samples. These data are then processed by the mineral liberation analysis (MLA) software in order to extract size and shape information, and combine, compare and group components for further examination. Automated data extraction provides highly representative measurement statistics devoid of manual work bias. The Cergowa sandstones were prepared for the analysis as non-granular samples in coated thin sections and granular samples in epoxy mounts. The former samples provide mineralogical data whereas the latter additionally generate textural parameters, both essential in interpretation of variability of flow competence. Comparisons between samples from an individual bed and between different beds of the measured sections give insights into the spatial and temporal flow development at a given locality. On the other hand, a comparison of different sections and regions of the formation will provide basis for the reconstruction of submarine flow events throughout the sedimentary basin and contribute to the characterisation of the provenance areas. Highly detailed quantitative data generated by this procedure have great potential in helping to recognise complex relationships between mineralogical and textural sorting by depositional processes.

**ZASTOSOWANIE ZAUTOMATYZOWANEJ MINERALOGII SEM DO KWANTYFIKACJI
MINERALNEGO I TEKSTURALNEGO WYSORTOWANIA OSADÓW
PODMORSKICH SPŁYWÓW GRAWITACYJNYCH**

Słowa kluczowe

skaningowy mikroskop elektronowy (SEM), zautomatyzowana mineralogia SEM, procesy depozycyjne, sortowanie osadów, podmorskie spływy grawitacyjne

Streszczenie

Zautomatyzowana mineralogia SEM jest analitycznym systemem bazującym na skaningowym mikroskopie elektronowym (SEM) wyposażonym w detektor elektronów wstecznie rozproszonych oraz spektrometr dyspersji energii (EDX). To zautomatyzowane narzędzie umożliwia kwantyfikację mineralogii, wielkości i geometrii komponentów ciał stałych. W artykule przedstawiono zastosowanie zautomatyzowanej mineralogii SEM w analizie mineralogicznego i teksturalnego sortowania osadów zdeponowanych przez podmorskie spływy grawitacyjne, na przykładzie piaskowców cergowskich (dolny oligocen) z polskich Karpat zewnętrznych. Analiza obrazów wysokiej rozdzielczości, generowanych przez elektrony wstecznie rozproszone (BSE), w połączeniu z zarejestrowanymi widmami EDX, pozwala określić fazy mineralne występujące w badanych próbkach. Te dane są następnie przetwarzane przez oprogramowanie *Mineral Liberation Analysis* (MLA) w celu ekstrakcji informacji o wielkości i kształcie komponentów, a także łączeniu, porównywaniu i grupowaniu wygenerowanych informacji do dalszych badań. Zautomatyzowana ekstrakcja danych dostarcza wysoce reprezentatywnych statystyk pomiarowych pozbawionych błędu pracy ręcznej. Piaskowce cergowskie zostały przygotowane do analizy jako zgłady w formie płytek cienkich oraz zatopione w żywicy wyseparowane ziarna. Pierwszy rodzaj próbek dostarcza danych o składzie mineralogicznym, natomiast drugi rodzaj dodatkowo pozwala wygenerować parametry teksturalne, oba istotne w interpretacji zmienności kompetencji podmorskich spływów grawitacyjnych. Porównania pomiędzy próbkami z tej samej warstwy oraz z różnych warstw profilu dają wgląd w przestrzenny i czasowy rozwój przepływu w danym miejscu. Natomiast porównanie próbek z różnych profili i regionów formacji dostarcza informacji do rekonstrukcji podmorskich przepływów grawitacyjnych w basenie sedymentacyjnym i przyczynia się do charakterystyki obszarów proveniencji. Wysoko szczegółowe dane ilościowe generowane w MLA mają duży potencjał w rozpoznaniu złożonych zależności pomiędzy mineralogicznym i teksturalnym sortowaniem przez procesy depozycyjne.

